Influence of Different Pole Head Shapes on Motor Performance in Switched Reluctance Motors

Mehmet POLAT, Ahmet YILDIZ
Department of Mechatronics Engineering, Faculty of Engineering, Firat University, Elazig, Turkey
ayildiz@firat.edu.tr

***Abstract*—The main reasons of the vibrations occurring in the stator of Switched Reluctance Motors (SRM) are the radial forces and they cause acoustic noise. This has an adverse effect on the performance of SRM. The aim of this study is to reduce radial forces by giving different geometric shapes to the pole heads and to investigate the effect of these pole shapes on the motor performance of SRM. In this study, the radial forces of four different SRMs having generally the same dimensions but different pole head shapes are calculated and compared with each other. In addition, the effects of different pole head shapes on the inductance curve and the torque ripple are investigated. To calculate the radial forces, torque and inductance values, ANSYS software is used which uses finite element method (FEM). After reshaping the pole heads, rotor position is changed with the increments of 1 degree from the unaligned to aligned position and the radial forces, torque and inductance values are calculated for each incremental position. According to the results, radial force is reduced about 19.03% at the rated current as compared to a standard SRM. However, torque ripple is observed to increase by about 3.29%.**

***Index Terms*—acoustic noise, inductance curve, radial force, switched reluctance motor, torque ripple.**

I. Introduction

SRMs are gaining more interest in recent years since they have simple and robust structure, ability to be controlled flexibly and high performance [1-5]. But there are still two main problems with the SRMs. First, when they are running, there is a noise due to the vibrations in torque and in radial forces. Second, the rotor position must be determined. Since the poles of the stator and rotor are salient, the air gap between the rotor and stator is variable. That's why the axial and radial forces acting on rotor poles vary continuously while the rotor is rotating. The most important ones of the magnetic reasons of the noise are the radial forces acting on the rotor. The forces acting on the rotor poles in the radial direction cause vibrations on the bearings. These vibrations may cause defections in the bearings after some period of time. It is possible to reduce the vibrations with some modifications in the design of the motor and in the control system. In the literature, there are many studies that describe how to reduce the noise and which source causes mostly the noise. A few has been performed by Cameron et al [6]. They mentioned the sources of the noise and effectiveness of each source (which source cause how much noise). In their study they determined some of the sources of the noise as the coincidence of the squares of the harmonics of the current and rotor resonance frequency harmonics, frequency of the excitation current and pulse width ratio. In another study, the experimental results in the case of single phase excitation while the rotor is in aligned position are compared with the results while the rotor is rotating. It has been shown that acoustic noise is greater in the aligned rotor position and the most effective reasons of the noise are the radial forces. It has also been shown experimentally that the other noise sources such as torque variations, the forces acting on the stator windings and mechanical asymmetry contribute to the acoustic noise less as compared to the radial forces [6, 7]. Tang Y. designed a 12 / 8 poles SRM to improve efficiency of the materials used and to reduce the noise. He performed magnetic analyses of the designed SRM, taking into account the nonlinearity, by using finite element and boundary element methods separately. He obtained radial forces acting on the rotor poles for different current values [8]. Cao et al. have proposed a novel solution that can be achieved direct force control and direct torque control synchronically. The proposed control method has been shown to reduce torque ripple and radial displacements of structure of single-winding bearingless Switched Reluctance Motors. They observed that radial displacement and torque ripple can be decreased by about 29% and 80%, respectively [9]. Ohdachi Y. designed optimum 3 – phase 6 / 8 poles SRM using dynamic FEM. He also optimized the shapes of the poles to minimize the torque ripples [10]. Koibuchi K. et al. performed basic design of SRM by using 2D FEM. The analyses of 6 / 4 poles SRM has been made numerically and using FEM. A two – switch classical driver circuit is used to drive the motor. One of the results of the study is the reduction in the torque ripples and increase in torque due to the enhancement of the stator pole arcs [11]. Pillay et al. investigated the vibrations in the SRM. They performed this investigation in the cases of salient and round stator poles. They showed that vibrations were more in the salient stator pole case [12]. Sanada M. et al. studied on new shapes of rotor poles to reduce the noise. The effects of various pole rates on the noise were investigated considering radial forces. As the number of poles increased, due to the reduction of the radial forces, the acoustic noise reduced. Then 6 types of rotor poles are defined due to the height of the rotor pole, for 3 – phase 6 / 4 SRM and the radial forces were investigated [13]. Anwar, M. N. and Iqbal, H. proposed an analytical method to detect the acoustic noise intensity and to calculate the radial force. The validity of the calculated radial force by using this analytical method was shown by the results calculated using FEM [14]. Miller,

Digital Object Identifier 10.4316/AECE.2020.03009

T.J.E. presented a detailed work on the design of an ideal SRM. An analytical method to predict the torque was proposed after presenting the general characteristics of the SRM. A magnetic simulation was performed using PC - SRD program then torque and energy equations were defined. Finally, the influence of the numbers of phases and poles on the acoustic noise was examined [15].

In this paper by giving new shapes to the stator and rotor pole heads it is aimed that the influences of the radial forces on the acoustic noise are reduced. In addition, the inductance curve and torque ripple of the SRM in case of saturated and unsaturated cases are examined. For this purpose, the radial forces, inductance curves and torque ripples of four SRMs with the generally same dimensions but different pole shapes are investigated and compared with each other. To calculate the radial forces, torque and inductance values, ANSYS software is used which uses finite element method (FEM). After reshaping the pole heads, rotor position is changed with the increments of 1° from the unaligned to aligned position and the radial forces, torque and inductance values are calculated for each incremental position.

II. The FEM Analyses of Designed Models

The main quantities calculated by FEM are the magnetic vector potential values. The relation between the magnetic vector potential and current density is given by Maxwell's equation as [16,17].

$$\nabla \times H = \nabla \times \left(\frac{1}{\mu} \nabla \times A \right) = J \tag{1}$$

where H is the magnetic field, J is the current density, A is the magnetic vector potential and μ is magnetic permeability. Equation (1) can be expressed in 2D analytically as;

$$\frac{\partial A}{\partial x}\left(\frac{1}{\mu} \frac{\partial A}{\partial x} \right) + \frac{\partial A}{\partial y}\left(\frac{1}{\mu} \frac{\partial A}{\partial y} \right) = -J \tag{2}$$

To solve (2), the region of solution is divided into adequate small elements such as triangles or rectangles.

In this study ANSYS software is used to obtain solutions. In FEM solution, Newton Raphson method is used for the nonlinear algebraic equations, while in the calculation of forces and torques Maxwell Stress Tensor method is employed [18].

Dirichlet boundary conditions are defined on the boundaries. In Maxwell stress tensor method, the local stress is calculated at all the boundary nodes of the surface and surface integral is taken to determine total tangential and normal components of the force. This method is preferred since it only needs one surface solution in the calculation of torque and magnetic force components in FEM. In 2D it is necessary to know the normal (radial) and tangential components of current density at any nodes through the closed contour when using Maxwell stress tensor method [19]. Stress components depend on the field components. The normal and tangential force and torque values on defined boundary line can be calculated by using (3-5) [20,21].

$$F_n = \frac{1}{2\pi\mu_0} \int_s \left(B_n^{\,2} - B_t^{\,2} \right) ds \tag{3}$$

$$F_t = \frac{1}{\mu_0} \int_s B_n B_t \, ds \tag{4}$$

$$T = \int_s \left[\frac{1}{\mu_0} \left(r \times B \right)\left(B \cdot n \right) - \frac{1}{2\mu_0} B^2 \left(r \times n \right) \right] ds \tag{5}$$

where μ_0 represents magnetic permeability, s is the surface, r is the position difference, B_t and B_n are the tangential and normal components of magnetic flux density, respectively, n is the normal vector of the surface, F_t and F_n are the tangential and normal components of the force, respectively, and T is the total produced torque [22-24].

The radial forces, inductance and torque curves of 4 SRMs which have the dimensions and other parameters as given in Appendix A, but their stator and rotor pole shapes different geometrically, are calculated and compared with each other.

Fig. 1 shows a standard SRM.

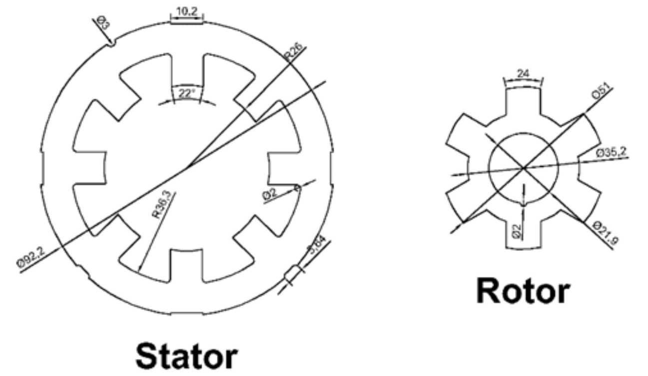

Figure 1. Front view of 8 / 6 poles SRM

In this study, four different SRM models are designed such that their motor dimension parameters are same except for the rotor and stator pole shapes. Their radial forces, torque and inductance values are calculated and are compared with each other. Standard SRM stator and rotor pole heads are chosen for the first model. The sharp edges of the pole heads of the first model are rounded to form the second model. The third and fourth models are designed similar to the standard SRM model, but they have different stator and pole heads.

III. Design Models of SRM

A standard 8 / 6 SRM is chosen for Model 1. The winding slot is rounded in order to provide maximum space for the windings and to have no space in that region. Fig. 2a shows this.

In Fig. 3a, 3D views of Model 1 from different directions are illustrated. As seen in Fig. 2b, the stator and rotor poles of Model 2 are rounded and its influence is investigated. Stator and rotor pole head geometries of Model 3 and 4 are designed with respect to air gap and pole head width. In this study, the design criteria used to reduce torque ripples in [25] is used to reduce radial forces.

Fig. 4 shows the reference shapes of stator and rotor poles. The parameters chosen for this geometry are given in Table I. Index g represents air gap. Fig. 2c illustrates Model

3 after the edges are rounded. The geometry of the stator and rotor poles of Model 4 is shown in Fig. 2d and 3D views from different directions are shown in Fig. 3b.

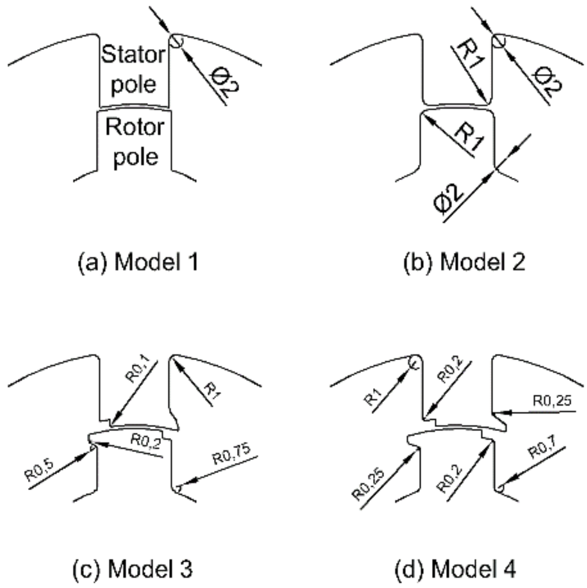

Figure 2. Stator and rotor pole shapes of models

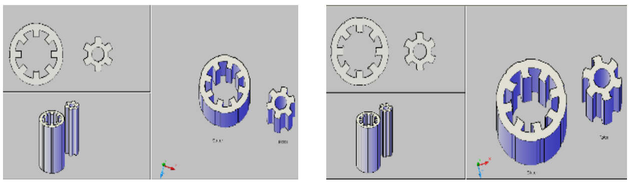

(a) Model 1 (b) Model 4

Figure 3. 3D views of Model 1 and Model 4 from different angles

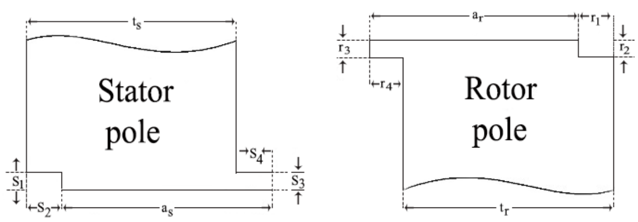

Figure 4. Reference shapes of stator and rotor poles

TABLE I. THE PARAMETERS RELATED TO THE POLE SHAPES OF MODEL 3 AND MODEL 4

	s_1	s_2	s_3	s_4	a_s	a_r	r_1	r_2	r_3	r_4
Model 3	2g	3.5°	4g	3.5°	22°	24°	3°	2g	4g	3°
Model 4	2g	4.5°	4g	4.5°	22°	24°	4°	2g	4g	4°

A. *Analysis of Models According to Radial Forces*

The variation of the radial force of Model 1, which is accepted as the most effective reason of the acoustic noise, with respect to the rotor position is given in Fig. 5a. To plot this curve, the rotor position is changed from unaligned to aligned with increments of one degree. The greatest radial force value is at aligned position and its value is 1550 N. The variation of radial force with respect to rotor angle is given in Fig. 5b for Model 2. A 3 N reduction in the force is determined from the graphics.

For Model 3, examination of Fig. 5c which shows radial force versus rotor position tells that the radial force is decreased considerably. Maximum radial force decreases to 1423 N. The decrease in radial force is 8.19% and 8.01% as compared to Model 1 and Model 2, respectively. Maximum radial force for Model 4 decreased to 1255 N as seen in Fig. 5d. According to this the radial force decreased by 19.03%, 18.87% and 11.8% as compared to Model 1, Model 2 and Model 3 respectively. Decrease of 19.03% in radial force with respect to standard model is a good result to reduce acoustic noise.

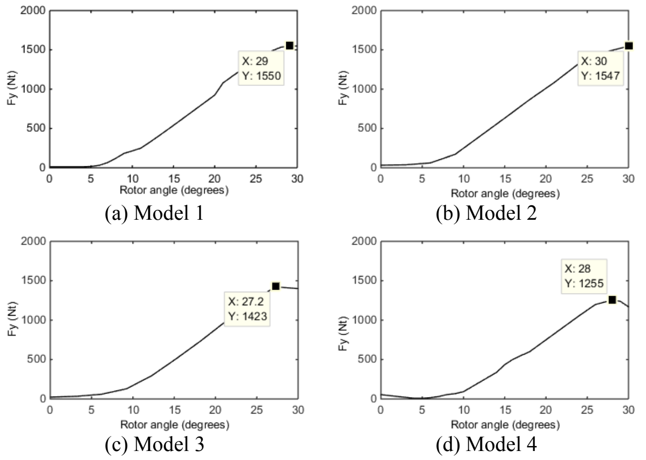

Figure 5. The radial force variations with respect to rotor position of models

The variations of radial force with respect to rotor position of all models are given in Fig. 6.

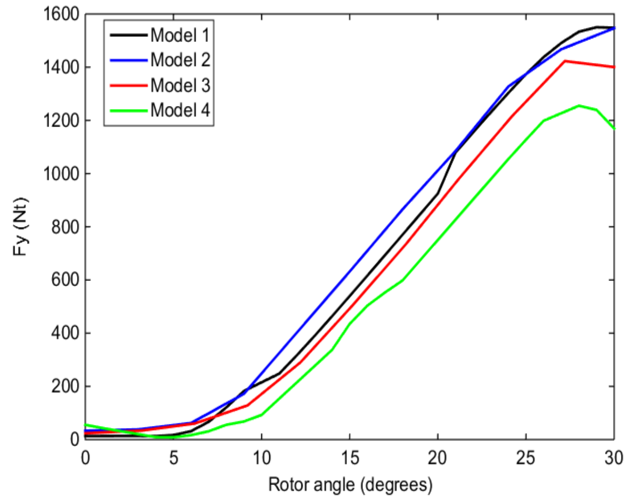

Figure 6. Radial force-rotor angle curves of all models

The comparison table of radial forces at aligned rotor position according to Model 1 is Table II.

TABLE II. THE RADIAL FORCES OF MODELS IN ALIGNED POSITION AND COMPARISON WITH MODEL 1

Models	**Radial Force (N)**	**Percentage decrease with respect to Model 1**
Model 1	1550	-
Model 2	1547	0.193
Model 3	1423	8.193
Model 4	1255	19.03

B. *Analysis of Models According to Torque Ripple and Inductance*

The torque curve of the Model 1 with respect to the rotor position at the rated current is shown in Fig. 7a. This curve has been obtained with the increments of 1° from the unaligned to aligned position. In order to determine the torque ripple from this curve, the maximum value (T_{max}) related to the torque curve of any phase and the value (T_{min}) which the torque curves intersect when passing from one phase to the other phase are obtained. Torque ripple can be calculated by using T_{max} and T_{min} values in (6) [26,27],

$$\%T_d = \frac{T_{\max} - T_{\min}}{T_{\max} + T_{\min}} * 100 \qquad (6)$$

For the graph shown in Fig. 7a, the torque ripple ratio of SRM has been calculated as about 5.13% by (6). This rate is about 36% in a standard three-phase SRM. The torque ripple ratio of Model 2 has been calculated as about 7.13% according to the torque curve in Fig. 7b depending on the rotor position at the rated current.

According to Model 1, the torque ripple rate increased by 2%. The torque ripple ratio of Model 3 has been calculated as about 8.7% according to the torque curve in Fig. 7c depending on the rotor position at the rated current.

According to the Model 1 and Model 2, the ripple ratio increased by 3.57% and 1.57%, respectively. The torque ripple ratio of Model 4 has been calculated as about 8.42% according to the torque curve in Fig. 7d depending on the rotor position at the rated current.

According to the Model 1 and Model 2, the ripple ratio increased by 3.29% and 1.29%, respectively and it decreased by 0.28% compared to Model 3.

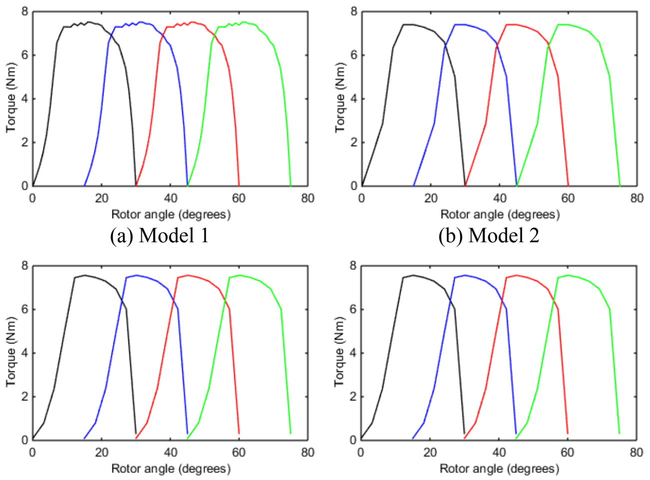

(a) Model 1 (b) Model 2
(c) Model 3 (d) Model 4

Figure 7. The variation of the torque with respect to rotor position of models

The variations of torque with respect to rotor position of all models are given in Fig. 8.

The variations of inductance curve of the Model 1 with respect to the rotor position at the rated current is given in Fig. 9a. L_{min}=6.333 mH and L_{max}=28.17 mH have been calculated by means of this curve.

The inductance change curve of the Model 2 with respect to the rotor position at the rated current is given in Fig. 9b. L_{min}=5.945 mH and L_{max}=27.394 mH have been calculated by means of this curve.

The inductance change curve of the Model 3 with respect to the rotor position at the rated current is given in Fig. 9c. L_{min}=6.948 mH and L_{max}=26.92 mH have been calculated by means of this curve. As shown in Fig. 9c, the symmetry in the inductance curves has been distorted and the slopes of rise and fall of the inductance is different according to the direction of rotation of the motor.

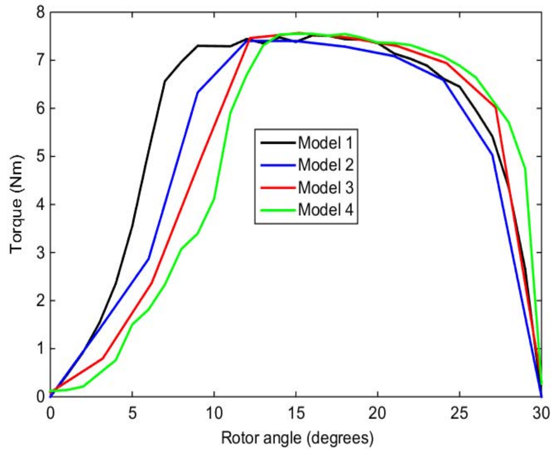

Figure 8. Torque - rotor angle curves of all models

The inductance change curve of the Model 4 with respect to the rotor position at the rated current is given in Fig. 9d. L_{min}=7.403 mH and L_{max}=26.31 mH have been calculated by means of this curve. As in Model 3, the symmetry in the inductance curves have been disappeared due to the asymmetry the stator and rotor poles.

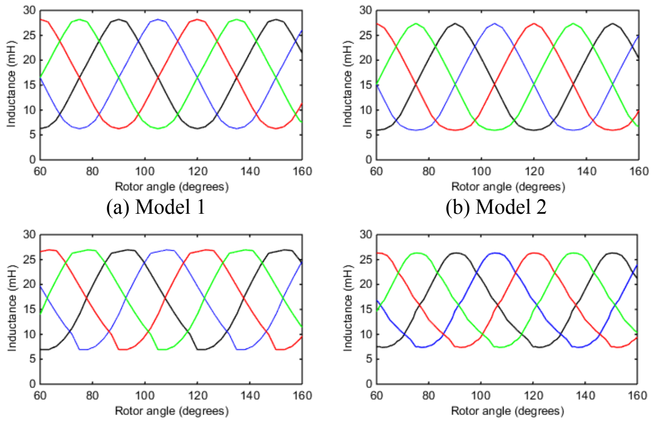

(a) Model 1 (b) Model 2
(c) Model 3 (d) Model 4

Figure 9. The variation of the inductance with respect to rotor position of models

By combining the results obtained above, Fig. 10 and Table III are obtained.

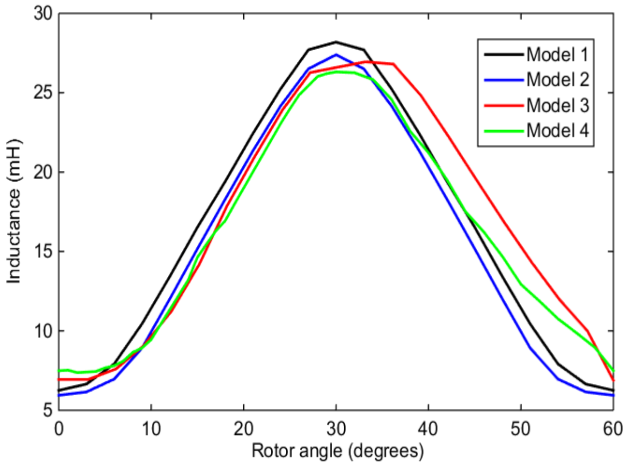

Figure 10. Inductance - rotor angle curves of all models

TABLE III. THE RIPPLE RATIO, NOMINAL TORQUE AND INDUCTANCE VALUES OF THE DESIGNED MODELS

Models	Torque Ripple (%)	Maximum Torque (Nm)	Inductance (mH)	
			L_{min}	L_{max}
Model 1	5.13	7.514	6.333	28.17
Model 2	7.13	7.400	5.945	27.39
Model 3	8.70	7.556	6.948	26.92
Model 4	8.42	7.545	7.403	26.31

IV. COMPARATIVE ANALYSIS OF MODEL 4

Operational characteristics in saturated and unsaturated cases of Model 4 have been investigated. Results of radial force, inductance curves and torque calculations are presented in comparison with standard type Model 1.

A. *Unsaturated Case*

In unsaturated operation the linear part of the magnetization curve of SRM is used. So, the SRM is operated at current values below the rated current. Radial forces, torque and inductance values are calculated while the rotor angle is changed from unaligned position to aligned position with the increments of one degree for current values of 3 A, 6 A and 9 A.

The variations of radial forces with respect to rotor position and current for unsaturated case of Model 1 and Model 4 are shown in Fig. 11.

It is determined that the radial force in the unsaturated case changes with almost the square of the value of current. Furthermore, the values of radial forces decreased considerably for Model 4 as compared to Model 1. These results are given in detail according to the current values in Table IV.

TABLE IV. COMPARISON OF RADIAL FORCES OF MODEL 1 AND MODEL 4 IN ALIGNED POSITION

Current (A)	3	6	9
	Radial Force (N)		
Model 1	120.30	473	1035
Model 4	97.22	376.5	819.9
Decrease in radial force with respect to Model 1 (%)	19.18	20.40	20.78

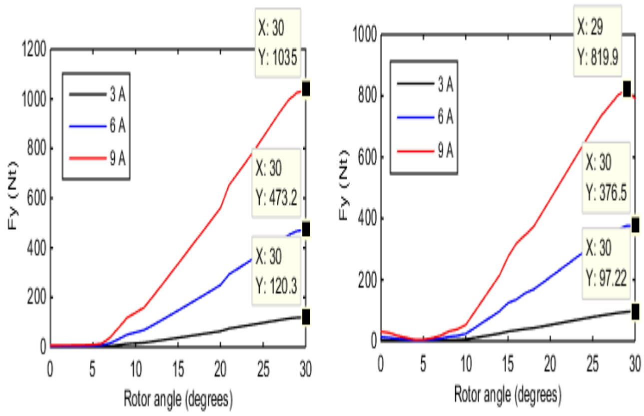

(a) Model 1 (b) Model 4

Figure 11. Radial force – rotor angle curves of the models in unsaturated operation

The variations of inductance curves of the Model 1 and Model 4 according to the rotor position and currents below the rated current are given in Fig. 12. As the inductance curves of Model 1 rise and fall on almost the same slope. Although the rise of inductance curves of the Model 4 is similar due to the asymmetry structure, it has been observed to follow different slopes in their fall, especially if we pay attention to the 9 A. In addition, it has been observed that Model 4 entered the saturation region at 9 A under the same operating conditions, unlike Model 1.

Also, the starting points of the rise have been changed. It has been observed that the inductance curves of Model 1 started to a linear rise at about 6 degrees. This value is approximately 9 degrees in Model 4. These results are important in the determination of transmission and cutting angles for the desired torque and the efficient operation of SRM.

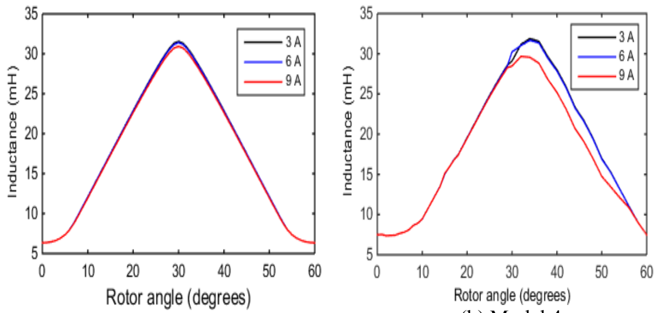

(a) Model 1 (b) Model 4

Figure 12. The variation of inductance depending on rotor position for different current values

The torques of the Model 1 and Model 4 according to the rotor position and currents under the rated current are given in Fig. 13. In order to reduce the torque ripple during the phase transitions, if the moments curve maintain its value until the next phase torque is activated and/or the next torque curve must rise rapidly when the previous torque curve is high. If these conditions are realized, the torque drop between phase transitions will not be high. Since the torque in the SRMs is changed depending on the square of the current, the torque increased as the current increased.

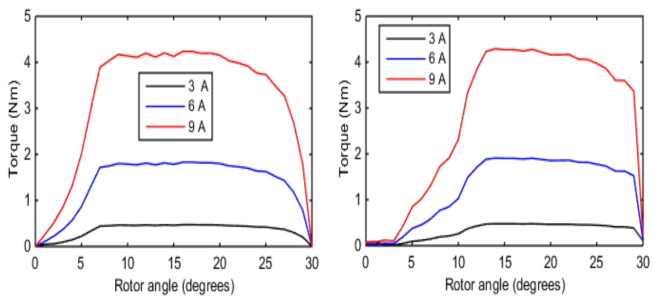

(a) Model 1 (b) Model 4

Figure 13. Torque – rotor angle curves of the models in unsaturated operation

When the torque curves in Model 1 were examined, it is observed that that the torque curves started to rise from the 0° and that the rise continued rapidly until 7°, then it reaches the peak values with the ripple, and the fall did not change much compared to the current values, and the starting point of the fall started at about 25° and ended at 30°. In Model 4, it is seen that the rise has started from 3° to 13° with the slight ripple, after that point it has ripple at the peak value and the fall does not change much according to the current values, and the starting point of the fall started at about 28°

and ended at 30°. Although the fall in Model 4 was sharper, the ripple ratio was slightly higher than Model 1 as previously mentioned due to the long rise.

B. Saturated Operation

As in the unsaturated operation, the rotor angle increased with one degree increments from unaligned to aligned position and radial forces, inductance curves and torque values are calculated at each step for the current values of 12, 15 and 18 A.

Radial force variations due to currents and rotor positions for Model 1 and 4 are given in Fig. 14 for saturated operation. In contrary to unsaturated operation, it can be said that the radial force variation is not so large. The values of the radial forces of Model 4 are also reduced considerably in comparison with Model 1, as in the unsaturated operation. These results are given in detail in Table V.

TABLE V. COMPARISON OF MODEL 1 AND MODEL 4 ACCORDING TO THEIR RADIAL FORCES IN THE ALIGNED POSITION

Current (A)	12	15	18
	Radial Force (N)		
Model 1	1550	1657	1723
Model 4	1255	1381	1430
Decrease in radial force with respect to Model 1 (%)	19.03	16.65	17.00

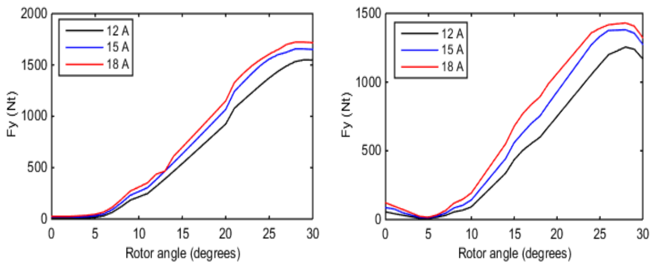

(a) Model 1 (b) Model 4

Figure 14. Radial force – rotor angle curves of the models in saturated operation

Inductance variations for saturation operation due to currents and rotor positions for Model 1 and Model 4 are given in Fig. 15. Since the inductance varies depending on both the phase and rotor current in the working zone where saturated is present, it shows a decreasing trend as the current increases. This case shows that the inductance in the saturation region is a function of both the winding current and the rotor angle.

Another result is that the inductance curves of Model 1 and Model 4 have risen and fallen on different slopes according to the current. However, for the same current value of Model 1, the rise and fall slopes of the inductance curve was the same but because of the asymmetric structure of Model 4, a different slope has been followed.

The starting point of the rise of inductances of Models 1 and Model 4 are different as in the unsaturated operation. This difference is almost the same as in the unsaturated region.

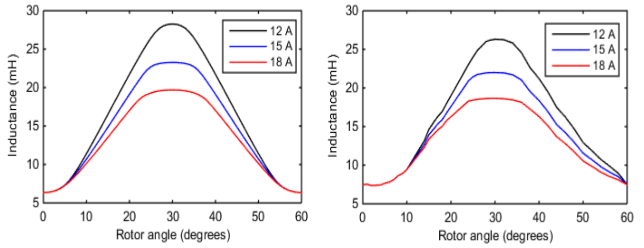

(a) Model 1 (b) Model 4

Figure 15. Inductance – rotor angle curves of the models in saturated operation

The variations of the torque of Model 1 and Model 4 according to the currents and rotor position for the saturated operation are given in Fig. 16. When the figures are examined, it is seen that the torque increases as the value of current increases. When the torque curves in Model 1 are examined, it is observed that the torque curves start to rise from the 0° and the rise is continued rapidly until 9°, after this point it holds at peak values with the ripple and the starting point of the fall started at approximately 25°, 23° and 20° according to 12 A, 15 A and 18 A current values, respectively and ended at 30°.

In Model 4, it is observed that the torque curves start to rise from 3° to 5° with slight ripple, after this angle it has ripple at the peak value and the starting point of the fall started approximately 26°, 24° and 22° according to 12 A, 15 A and 18 A current values, respectively and ended point at 30°.

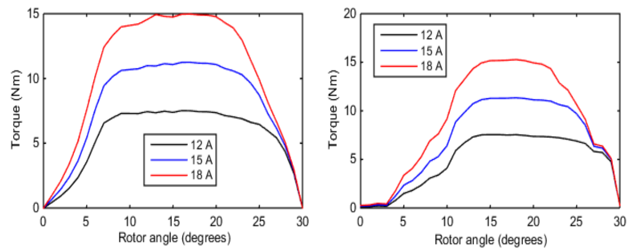

(a) Model 1 (b) Model 4

Figure 16. Torque – rotor angle curves of the models in saturated operation

The comparative results of Model 1 and Model 4 at the rated current condition are given in Table VI.

TABLE VI. THE COMPARATIVE RESULTS OF MODEL 1 AND MODEL 4

Models	**Radial Force (N)**	**Maximum Torque (Nm)**	**Ripple Ratio (%)**	**Decrease in radial forcewith respect to Model 1 (%)**	**Increase in ripple ratio with respect to Model 1 (%)**
Model 1	1550	7.514	5.13	-	-
Model 4	1255	7.545	8.42	19.03	3.29

According to the comparative results, the radial force of the Model 4 decreased by approximately 19.03% compared to Model 1. However, the torque ripple ratio of Model 4 increased by 3.29% compared to Model 1. In addition, it has been observed that the maximum torque value of both models is approximately the same.

V. CONCLUSION

In this paper, the effects of the stator and rotor pole shapes on the performance of the Switched Reluctance Motor are investigated.

Basically, three parameters are emphasized. These parameters are radial forces, inductance curve and torque ripple, respectively. To reduce the radial forces causing acoustic noise, the stator and rotor pole heads are given different geometrical shapes.

Radial force is reduced approximately 19.03% at the rated current as compared to a standard SRM. However, torque ripple is observed to increase by approximately 3.29%.

It has been observed that the inductance slopes change according to the different rotor and stator pole shapes. In addition, it has been observed that the inductance values in the aligned position differed with the inductance values in the unaligned and accordingly the L_{min} and L_{max} values have been changed. These inductance changes will have effect on the generated torque. In addition, the points where the inductances begin to rise changed. These cases should be considered when calculating the trigger angles of the motors to ensure good performance.

According to the results it can be said that some modifications may be done to control radial forces, inductance curves and torque ripple in design phase.

APPENDIX A

General properties of the designed SRMs:

Structural parameters	Value	Structural parameters	Value
Number of stator poles (Ns)	8	Stator inner diameter (mm)	52
Number of rotor poles (Nr)	6	Stator pack length (mm)	180
Length of stator pole arc (°)	22	Shaft diameter (mm)	22
Length of rotor pole arc (°)	24	Rotor outer diameter (mm)	51
Stator pole width (mm)	9.98	Stator pole length (mm)	10.1
Rotor pole width (mm)	10.9	Rotor pole length (mm)	7.9
Stator pole pitch (°)	45	Number of turns per phase	108
Rotor pole pitch (°)	60	Diameter of the wires (mm)	0.75
Air gap (mm)	0.5	Rated current (A)	12
Stator outer diameter (mm)	92.2		

REFERENCES

[1] E. El-Kharashi, H. Hassanien, “Reconstruction of the switched reluctance motor stator,” Journal of Electrical Engineering, vol. 63, no. 1, pp. 3-12, 2012. doi: 10.2478/v10187-012-0001-2

[2] A. Yıldız, M. Polat, “Investigation of the effect of stator and rotor pole ratios on torque and efficiency in Inverted Switched Reluctance Motor,” Journal of Engineering and Technology, vol. 3, no. 1, pp. 12-24, 2019.

[3] E. K. Beser, S. Camur, B. Arifoglu, E. Beser, "Design and Analysis of an Axially Laminated Reluctance Motor for Variable-Speed Applications," Advances in Electrical and Computer Engineering, vol.13, no.1, pp.75-80, 2013. doi:10.4316/AECE.2013.01013

[4] K. Wrobel, K. Tomczewski, "Effect of Objective Function Formulation on Static and Operating Parameters of a Switched Reluctance Motor After Optimization of Magnetic Circuit Shape," Advances in Electrical and Computer Engineering, vol.18, no.3, pp.23-28, 2018. doi:10.4316/AECE.2018.03004

[5] A. Yıldız, M. Polat, M. T. Özdemir, "Design Optimization of Inverted Switched Reluctance Motor using Ant Colony Optimization Algorithm," 2018 International Conference on Artificial Intelligence and Data Processing (IDAP), Malatya, Turkey, 2018. doi: 10.1109/IDAP.2018.8620923

[6] D.E. Cameron, J.H. Lang, S.D. Umans, “The origin of acoustic noise in variable-reluctance motors,” Conference Record of the IEEE Industry Applications Society Annual Meeting, San Diego, USA, 01-05 October 1989. doi: 10.1109/IAS.1989.96638

[7] D.E. Cameron, J.H. Lang, S.D. Umans, “The origin of acoustic noise in variable-reluctance motors,” IEEE Transaction on Industry Applications, vol. 28, no. 6, pp. 1250-1255, 1992. doi: 10.1109/28.175275

[8] Y. Tang, “Characterization, numerical analysis, and design of switched reluctance motors,” IEEE Transactions on Industry Applications, vol. 33, no.6, pp. 1544-1552, 1997. doi: 10.1109/28.649967

[9] X. Cao, Q. Liu, H. Zhou, Z. Deng, “Direct control of torque and levitation force for dual-winding bearingless switched reluctance motor,” Electric Power Systems Research, vol. 145, pp. 214-222, 2017. doi: 10.1016/j.epsr.2017.01.015

[10] Y. Ohdachi, Y. Kawase, Y. Miura, Y. Hayashi, “Optimum design of switched reluctance motors using dynamic finite element analysis,” IEEE Transaction on Magnetics, vol. 33, no. 2 pp. 2033–2036, 1997. doi: 10.1109/20.582709

[11] K. Koibuchi, T. Onho, K. Sawa, “A basic study for optimal design of switched reluctance motor by finite element method,” IEEE Transaction on Magnetics, vol. 33, no. 2 pp. 2077–2080, 1997. doi: 10.1109/20.582726

[12] P. Pillay, W. Cai, “An investigation into vibration in switched reluctance motors,” IEEE Transactions on Industry Applications, vol. 35, no. 3, pp. 589– 596 1999. doi: 10.1109/28.767007

[13] M. Sanada, S. Morimoto, Y. Takeda, N. Matsui, “Novel rotor pole design of switched reluctance motors to reduce the acoustic noise,” Conference Record of the 2000 IEEE Industry Applications Conference, Thirty-Fifth IAS Annual Meeting and World Conference on Industrial Applications of Electrical Energy, Rome, Italy, 08-12 October 2000. doi: 10.1109/IAS.2000.881033

[14] M.N. Anwar, O. Husain, “Radial force calculation and acoustic noise prediction in switched reluctance machines,” IEEE Transactions on Industry Applications, vol. 36, no. 6, pp. 589– 1597, 2000. doi: 10.1109/28.887210

[15] T.J.E. Miller, “Optimal design of switched reluctance motors,” IEEE Transaction on Industrial Electronics, vol. 49, no. 1, pp. 15– 27, 2002. doi: 10.1109/41.982244

[16] R. Brambilla, F. Grilli, L. Martini, M. Bocchi, G. Angeli, “A finite-element method framework for modeling rotating machines with superconducting windings,” IEEE Transactions on Applied Superconductivity, vol. 28, no. 5, pp. 1-11, 2018. doi: 10.1109/TASC.2018.2812884

[17] A. Jabbari, “Exact analytical modeling of magnetic vector potential in surface inset permanent magnet DC machines considering magnet segmentation,” Journal of Electrical Engineering, vol. 69, no. 1, pp. 39-45, 2018. doi: 10.1515/jee-2018-0005

[18] S. Hartmann, “A remark on the application of the Newton-Raphson method in non-linear finite element analysis,” Computational Mechanics, vol. 36, no. 2, pp. 100-116, 2005. doi: 10.1007/s00466-004-0630-9

[19] M. Moallem, C.M. Ong, L.E. Unnewehr, “Effect of rotor profiles on the torque of a switched reluctance motor,” IEEE Transactions on Industry Applications, vol. 28, no. 2, pp. 364-369, 1992. doi: 10.1109/28.126743

[20] D. Zarko, D. Ban, and T. A. Lipo, “Analytical solution for cogging torque in surface permanent-magnet motors using conformal mapping”, IEEE Transactions on Magnetics, vol. 44, no.1, pp. 52-65, 2008. doi: 10.1109/TMAG.2007.908652

[21] M. Moallem, C.M. Ong, “Predicting the torque of a switched reluctance machine from its finite element field solution,” IEEE Transactions on Energy Conversion, vol. 5, no. 4, pp. 733-739, 1990. doi: 10.1109/60.63147

[22] M. Abbasian, M. Moallem, B. Fahimi, “Double-stator switched reluctance machines (DSSRM): Fundamentals and magnetic force analysis,” IEEE Transactions on Energy Conversion vol. 25, no. 3, pp. 589-597, 2010. doi: 10.1109/TEC.2010.2051547

[23] C. Lee, R. Krishnan, “New designs of a two-phase E-core switched reluctance machine by optimizing the magnetic structure for a specific application: Concept, design, and analysis,” IEEE Transactions on Industry Applications, vol. 45, no. 5, pp. 1804-1814, 2009. doi: 10.1109/TIA.2009.2027570

[24] W. Zhu, B. Fahimi, S. Pekarek, "A field reconstruction method for optimal excitation of permanent magnet synchronous machines," IEEE Transactions on Energy Conversion, vol. 21, no. 2, pp. 305-313, 2006. doi: 10.1109/TEC.2005.859979

[25] M. Galip, Y. Ozoglu, E. Mese, "An approach to torque ripple reduction in fully pitched switched reluctance motors by pole tip shaping," 11th IEEE Mediterranean Electrotechnical Conference, Cairo, Egypt, 07-09 May 2002. doi: 10.1109/MELECON.2002.1014550

[26] J. H. Lee, E. W. Lee, J. H. Kim, D. J. Lee, "Design of the single phase SRM considering the torque ripple," 2005 International Conference on Power Electronics and Drives Systems, Kuala Lumpur, Malaysia, 2005. doi: 10.1109/PEDS.2005.1619865

[27] Y. Fan, K. T. Chau, "Torque ripple minimization of four-phase doubly salient permanent magnet motors using two-phase operation," Electric Power Components and Systems, vol. 28, no.4, pp. 401-415,2006. doi: 10.1080/15325000500346701